Journal of Electronic Imaging 9(1), 22–31 (January 2000).

Comparison of adaptive linear interpolation and conventional linear interpolation for digital radiography systems

Fang Xu*
Hong Liu*
Ge Wang**
Bennett A. Alford
University of Virginia
MR-4 Building, Room 1157
Charlottesville, Virginia 22908

Abstract. *Some large field digital radiography systems are currently under development using multiple detectors. These small size two dimension detectors are abutted together to cover a large field. Physical gaps existing between adjacent detectors produce seams between the resultant subimages. In this paper, an adaptive linear interpolation algorithm was introduced for estimating missing information at the seams and was compared with conventional linear interpolation and with nonlinear interpolation. The effectiveness of the algorithms was evaluated for relative/absolute errors. Phantom images were acquired using prototype digital radiography systems. Seams with width ranging from two pixel to six pixel were introduced and adaptive linear interpolation algorithms were applied to estimate missing information at the seams. Quantitatively, the adaptive interpolation offers at least equivalent or less error than that of the linear interpolation algorithm. The experimental results prove that there is a significant difference between two algorithms for tested radiographic images. The comparison results also show that the adaptive interpolation offers better performance than nonlinear interpolation. When developing large field digital radiography imaging systems, gaps between adjacent detectors should be minimized. For narrow seams, the adaptive linear interpolation algorithm is a practical solution because of its simplicity and effectiveness.* © *2000 SPIE and IS&T.* [S1017-9909(00)00201-4]

1 Introduction

Various electronic imaging techniques were investigated recently for digital radiography.[1–5] Due to constraints of current technology, some electronic imaging systems cover a large field but with a relatively low spatial resolution. Current high spatial resolution detectors, such as charge coupled devices (CCDs) can only cover a small field (usually less than 10 cm×10 cm). In order to acquire a large field digital radiograph with high spatial resolution, scanning apparatus or multiple detector designs are investigated.[6–9] Some prototype systems are comprised of multiple small sized electronic detectors, which are abutted together[10] (Fig. 1). Each detector produces a subimage corresponding to part of the object imaged. By combining the subimages, a full field view of the object is created. However, the resultant image will contain seams between the subimages produced by the gaps between the abutted detectors. Information located in the seams is lost. The missing information can be estimated using mathematical interpolation to model the known data and to evaluate this function at the missing data points. Thus, missing data (pixel values) are estimated using their surrounding pixel values. Interpolation algorithms assume that the physical characteristics and attributes of the missing data are most accurately reflected from local, rather than distant pixel values.

The results of our previous studies indicated that when the seams are narrow, a well-designed interpolation algorithm can effectively fill the seams between subimages.[11] No distracting artifact exits to draw the attention from the reviewers. Further, the simple linear interpolation algorithms offer similar accuracy as more complicated nonlinear algorithms, such as polynomial and cubic spline interpolations. When the seam size becomes wider, the errors and geometrical distortions introduced by interpolation algorithms get much higher and noticeable. In this paper, we report our study of developing an optimized linear interpolation technique: adaptive linear interpolation. We applied the adaptive interpolation to digitally acquired phantom images. The effectiveness of the adaptive interpolation was compared with conventional local weighting interpolation, for various seam widths. *In addition, it was also compared with nonlinear interpolation.*

*Current address: Johns Hopkins University, 310A Traylor, 720 Rutland Ave., Baltimore, MD 21205. E-mail: Hliu@jhmi.edu

**Current address: University of Iowa.

Paper 980225 received June 8, 1998; revised manuscript received June 24, 1999; accepted Sep. 24, 1999.
1017-9909/2000/$15.00 © 2000 SPIE and IS&T.

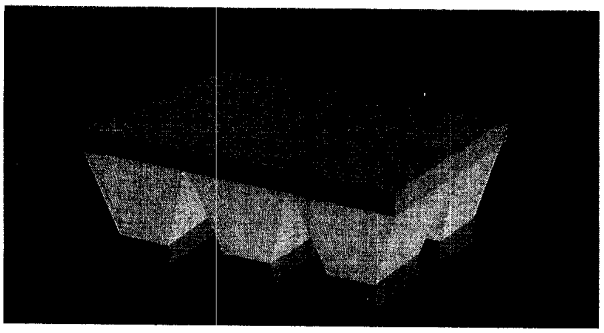

Fig. 1 Example of digital radiography system using multiple detectors.

2 Theory

2.1 *Linear Local Weighting*

Conventional linear interpolation, also called local weighting interpolation, using a finite number of nearest neighbor points gives interpolated values without continuous first or higher order derivatives. Although the mathematical result is a discontinuity in the interpolated function, if we assume the local nearest neighbor points have more common attributes with the missing data than other points in the image, local weighting approaches have validity. When doing local weighting interpolation, we also employ the weighting factor concept to assign coefficients to known data points based on their location relative to the missing data points (i.e., closer points have larger weighting coefficients). Generally, the interpolation between N points has the following formula:

$$\text{out}=\sum_{i=1}^{N} w_i^* \text{input}_i, \tag{1}$$

where w_i are weighting factors and input_i are the local pixel values used. Typically, the value of w_i ranges from 0 to 1 and the sum of all weighting factors is 1. As discussed above, we assign the weighting factors based on the distance rule with closer points having larger weighting factors expressed as:

$$w_i=\frac{\frac{1}{d_i}}{\sum_{i=1}^{N}\frac{1}{d_i}}, \tag{2}$$

where d_i is the distance from the ith neighbor point to the missing data and the smaller the d_i, the larger the weighting factor.

2.2. *Adaptive Linear Interpolation*

Adaptive linear interpolation is developed on the basis of linear local weighting interpolation algorithm. Here we first choose a group of known pixels that are very close to the unknown pixel. Then we find another group of pixels which has the smallest Euclidean distance to the first group. Last, we choose two pixels from these two groups, respectively, and use them to interpolate the unknown pixels (by linear local weighting interpolation). The mathematical model used in our investigation is described in detail in the following section.

Table 1 Illustration of known pixels and the pixels to be interpolated.

	254	255	256	257
$i-1$	$B(i-1,254)$	$A'(i-1,255)$	$A'(i-1,256)$	$C(i-1,257)$
i	$B(i,254)$	$A'(i,255)$	$A'(i,256)$	$C(i,257)$
$i+1$	$B(i+1,254)$	$A'(i+1,255)$	$A'(i+1,256)$	$C(i+1,257)$

3 Methods

3.1. *Radiographic Image Acquisition*

A series of phantom images acquired from two digital radiography systems (a fiber optically coupled CCD[7] and a lens coupled CCD) were used in these experiments. The phantom images were acquired with factors used in clinical radiation. Before applying any interpolation algorithms, the pixel values of the digital image were manipulated by a mathematical procedure, usually called flat fielding, to correct the vignetting effect introduced by lens, optical fiber and other components in the optoelectronic imaging chain.[2] Therefore, the profile of a uniform object on either side of the seam is flat for interpolation.

3.2 *Application of Adaptive Linear Interpolation to Digital Bone Images*

In order to examine the effectiveness of both linear and adaptive interpolation algorithms, seams of various widths were introduced to the phantom images. The following describes the method used to introduce a two-pixel wide seam. In this investigation, seams with widths ranging from two-pixel wide to six-pixel wide are introduced with similar method.

For convenience, a 512 by 512 pixel array ($64\,\mu m \times 64\,\mu m$ pixels), which is a portion of the original digital image, was used (A) (see Table 1). This image was divided into two subimages (B and C). From image A we constructed subimage B (left half of A) without the rightmost column and subimage C (right half of A) without the leftmost column. That is, $B(i,j)=A(i,j)$, $C(i,J)=A(i,j+257)$, where i is from 0 to 511, j is from 0 to 254. B and C were then abutted to a new 512 by 512 image with a two-pixel wide vertical seam at the center of the image. An interpolation algorithm can be applied to fill the gap, resulting in an interpolated image (A'). Our adaptive interpolation algorithm is explained as follows.

Generally speaking, structures of interest in the field of view are oriented arbitrarily. The seam typically transverses available data at an oblique angle. As a result, the profile of available data on one side of the seam is the most similar to a shifted version of the profile of known data on the other side of the seam. Therefore, interpolation along the inclined paths defined by the relative shift of the two profiles should produce minimum image blurring in recovery of the missing gap.

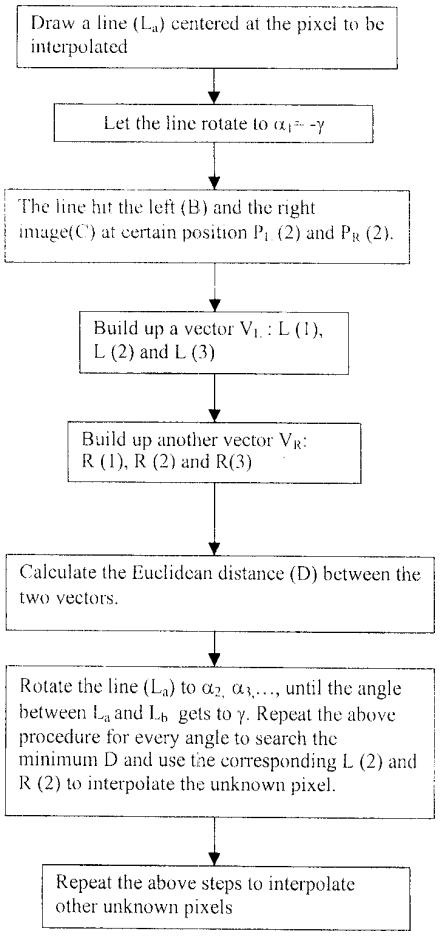

Fig. 2 Flow chart to illustrate the adaptive linear interpolation.

Referring to Figs. 2 and 3, to estimate pixel $A'(i, 255)$, we can draw a number of lines that make angles α with respect to the horizontal direction, say α ranging from $-\pi/3$ to $\pi/3$, each of such lines hits the left (B) and right (C) images at position $P_{L(2)}$ and $P_{R(2)}$. Then we have two

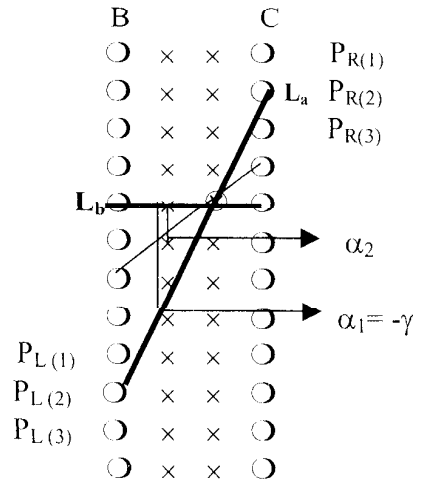

Fig. 3 Schematic to show the principle of adaptive interpolation.

vectors V_L and V_R centered at $P_{L(2)}$ and $P_{R(2)}$, respectively. (We use linear local weighting interpolation if the coordinates of $P_{L(2)}$ and $P_{R(2)}$ are not integers.) A segment of the data profile on the left side of the seam, for example, $L(1)=B(k-1,254)$, $L(2)=B(k,254)$ and $L(3)=B(k+1,254)$, are matched to a counterpart on the right side of the seam. This is done by minimizing the Euclidean distance between the two vectors corresponding to the two data segments. The Euclidean distance D is expressed as

$$D=\sqrt{[L(1)-R(1)]^2+[L(2)-R(2)]^2+[L(3)-R(3)]^2}, \tag{3}$$

where $D=D_{\min}$, $L_{\min}\Leftarrow L(2)$, and $R_{\min}\Leftarrow R(2)$. Finally, $L_{\min}$ and $R_{\min}$ are linearly combined to interpolate $A'(i,255)$:

$$A'(i,255)=\frac{\frac{1}{d_{L_{\min}}}L_{\min}+\frac{1}{d_{R_{\min}}}R_{\min}}{\frac{1}{d_{L_{\min}}}+\frac{1}{d_{R_{\min}}}}, \tag{4}$$

where $d_{L_{\min}}=1$, $d_{R_{\min}}=2$, which are the distances from pixel $A'(i,255)$ to $P_{L(2)}$ and $P_{R(2)}$, respectively.

4 Experimental Results

4.1 *Errors Introduced by Interpolation*

The effectiveness of the interpolation algorithm is evaluated quantitatively using two "error" concepts. They are:

$$\text{Error1}=\frac{\sum_{i=1}^{N}|x_0-x_p|}{N}, \tag{5}$$

$$\text{Error2}=\frac{\sum_{i=1}^{N}\frac{|x_0-x_p|}{x_0}}{N}. \tag{6}$$

Here x_0 is the original true pixel value and x_p is the interpolated value. N is the total number of the pixels in the seam. Error 1 is the average absolute error and Error 2 is the average relative error.

In our investigation, seams with a width ranging from two-pixel wide to six-pixel wide were introduced to a series of phantom images. Both adaptive interpolation and conventional linear interpolation algorithms were applied to these images. Errors induced by the algorithms were calculated using the formulas given above. The results are shown in Tables 2–5.

The errors given in Table 2 were calculated from a phantom image, as shown by Fig. 4(a). The image was acquired using a digital radiography prototype with factors used in clinical radiation. Before the seams were introduced and the interpolation algorithms were applied, a 512×512 subarray was cropped. Refer to Fig. 4 for the original image without seam, the image with seam, and the images interpolated with adaptive and conventional algorithms.

Table 2 Comparison of adaptive and conventional linear interpolation, a phantom image of hand.

	Error1					Error2				
Method\Seam width	2 pixels	3 pixels	4 pixels	5 pixels	6 pixels	2 pixels	3 pixels	4 pixels	5 pixels	6 pixels
Local weighting linear interpolation	5.5970	5.6680	5.8434	5.9586	6.2547	0.0902	0.0881	0.0924	0.0939	0.0983
Adaptive linear interpolation	5.3656	5.2962	5.5969	5.6656	5.9049	0.0860	0.0874	0.0912	0.0920	0.0980

Table 3 Comparison of adaptive and conventional linear interpolation, a phantom image of hand.

	Error1					Error2				
Method/Seam width	2 pixels	3 pixels	4 pixels	5 pixels	6 pixels	2 pixels	3 pixels	4 pixels	5 pixels	6 pixels
Local weighting linear interpolation	4.8939	5.3685	5.6889	5.8793	5.9801	0.0417	0.0470	0.0512	0.0529	0.0543
Adaptive linear interpolation	4.9064	4.9399	5.1347	5.2967	5.5225	0.0429	0.0448	0.0475	0.0498	0.0541

Table 4 Comparison of adaptive and conventional linear interpolation, a phantom image of wrist.

	Error1					Error2				
Method/Seam width	2 pixels	3 pixels	4 pixels	5 pixels	6 pixels	2 pixels	3 pixels	4 pixels	5 pixels	6 pixels
Local weighting linear interpolation	4.9495	5.2435	5.6534	5.9779	6.2519	0.0974	0.1013	0.1076	0.1150	0.1198
Adaptive linear interpolation	4.5507	5.2581	5.3763	5.6658	5.5421	0.0862	0.1011	0.1032	0.1090	0.1062

Table 5 Comparison of adaptive and conventional linear interpolation, a phantom image of forearm.

	Error 1					Error 2				
Method/Seam width	2 pixels	3 pixels	4 pixels	5 pixels	6 pixels	2 pixels	3 pixels	4 pixels	5 pixels	6 pixels
Local weighting linear interpolation	3.9163	3.9463	4.0962	4.1524	4.0538	0.0889	0.0902	0.0939	0.0956	0.0936
Adaptive linear interpolation	3.7865	3.7927	3.8800	3.9272	3.8949	0.0851	0.0867	0.0887	0.0899	0.0894

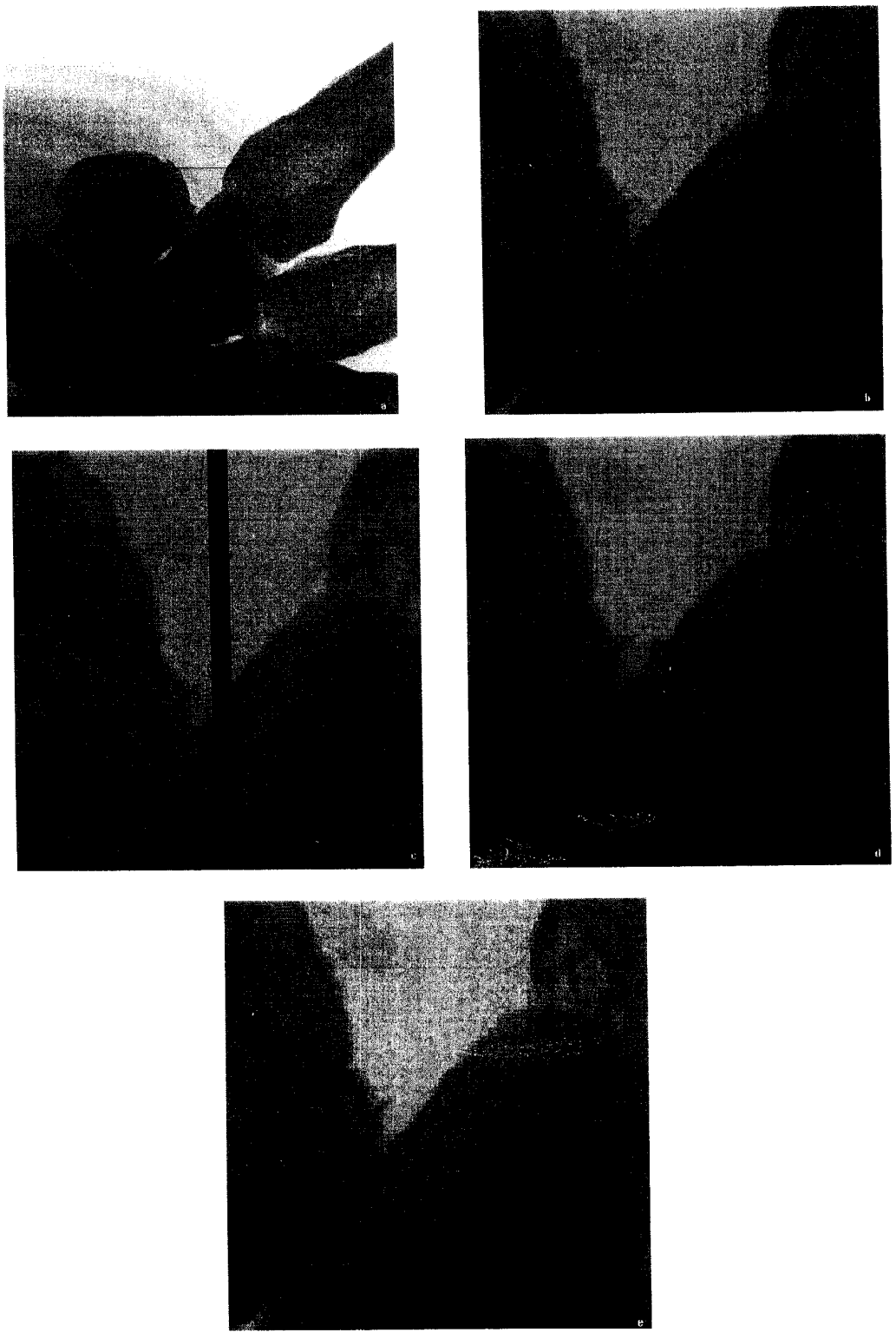

Fig. 4 This is a hand bone phantom image. The original image was acquired with factors used in clinical radiation, (a) original image with the portion to be enlarged in the rectangular block; (b) area of interest without seam (enlarged); (c) area of interest with six-pixel seam (enlarged); (d) area of interest reconstructed by linear local weighting interpolation (enlarged); (e) area of interest reconstructed by adaptive linear interpolation (enlarged).

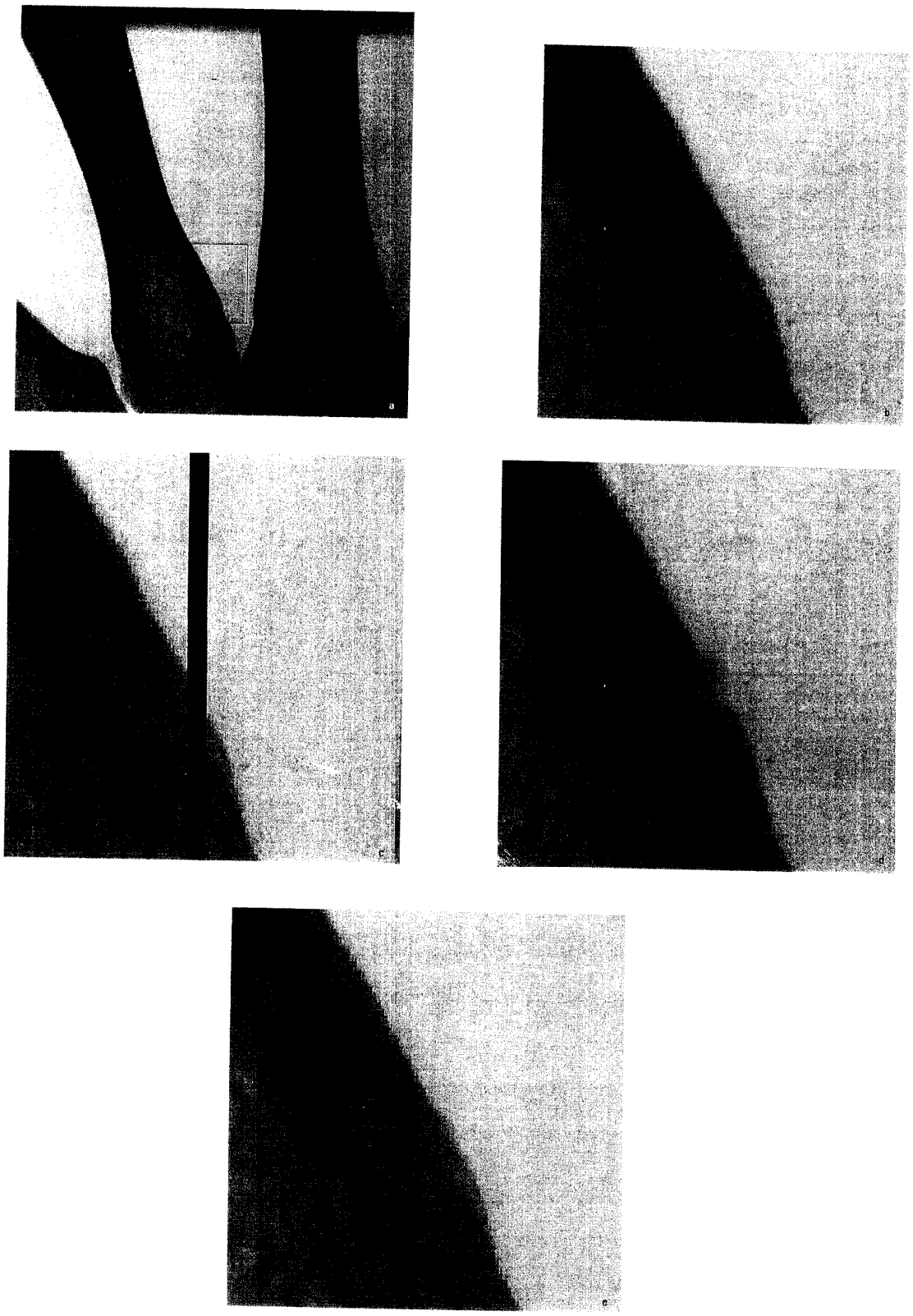

Fig. 5 This is a hand bone phantom image. The original image was acquired with factors used in clinical radiation, (a) original image with the portion to be enlarged in the rectangular block; (b) area of interest without seam (enlarged); (c) area of interest with six-pixel seam (enlarged); (d) area of interest reconstructed by linear local weighting interpolation (enlarged); (e) area of interest reconstructed by adaptive linear interpolation (enlarged).

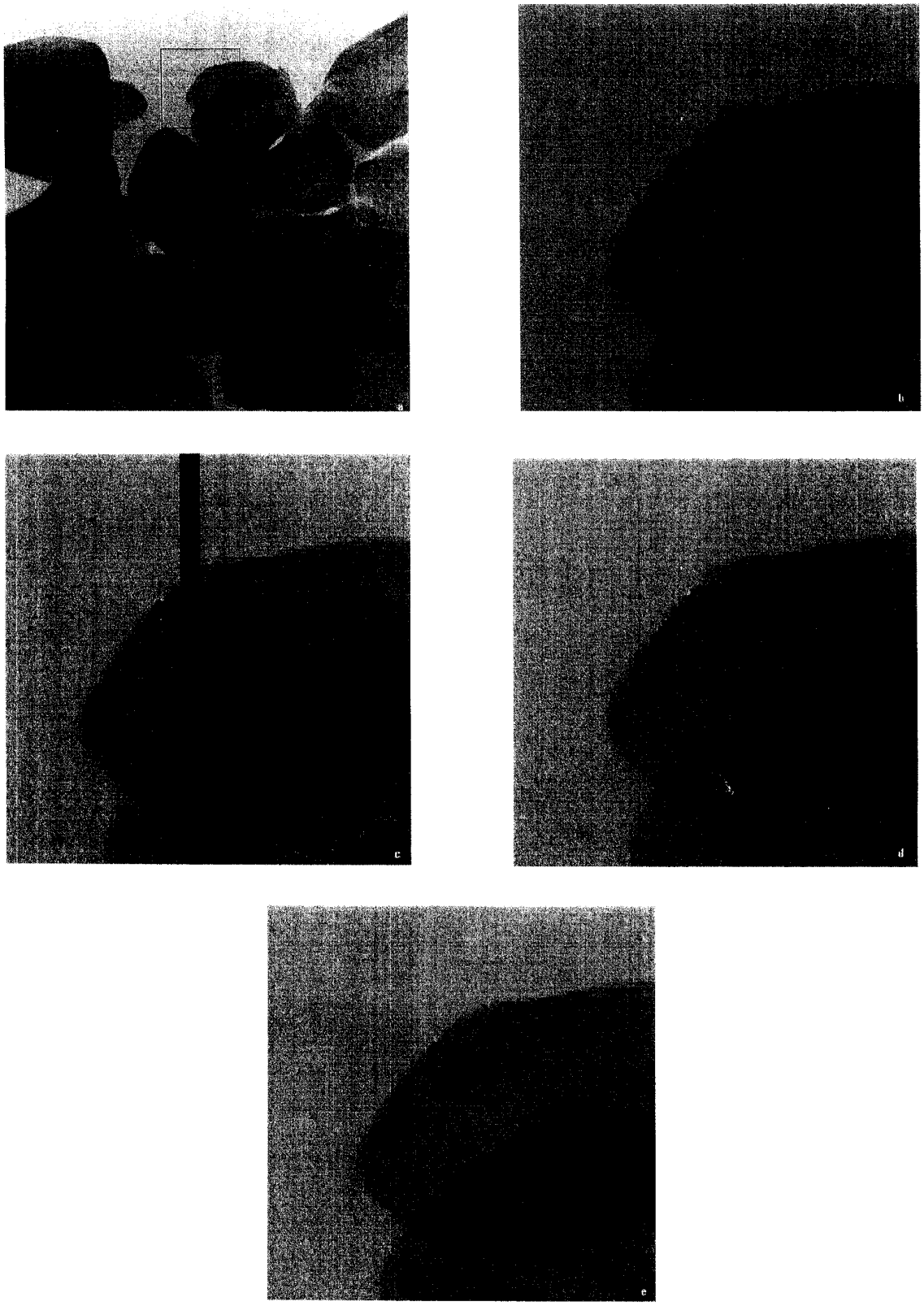

Fig. 6 This is a wrist bone phantom image. The original image was acquired with factors used in clinical radiation, (a) original image with the portion to be enlarged in the rectangular block; (b) area of interest without seam (enlarged); (c) area of interest with six-pixel seam (enlarged); (d) area of interest reconstructed by linear local weighting interpolation (enlarged); (e) area of interest reconstructed by adaptive linear interpolation (enlarged).

Table 6 Mean value of relative errors introduced by adaptive interpolation for each seam width and confidence interval of the mean.

Seam width	Mean (absolute error)	Mean (relative error)
2	4.6523	0.075 050
3	4.8217	0.080 000
4	4.9970	0.082 650
5	5.1388	0.085 175
6	5.2161	0.091 125

The errors given in Table 3 were calculated from a phantom image, as shown by Fig. 5(a). The image was acquired using a digital radiography prototype with factors used in clinical radiation. Before the seams were introduced and the interpolation algorithms were applied, a 512×512 subarray was cropped. Refer to Fig. 5 for the original image without seam, the image with seam, and the images interpolated with adaptive and conventional algorithms.

The errors given in Table 4 were calculated from a phantom image, as shown by Fig. 6(a). The image was acquired using a digital radiography prototype with factors used in clinical radiation. Before the seams were introduced and the interpolation algorithms were applied, a 512×512 subarray was cropped. Refer to Fig. 6 for the original image without seam, the image with seam, and the images interpolated with adaptive and conventional algorithms.

The errors given in Table 5 were calculated from a phantom image. It was acquired using a digital radiography prototype under clinical radiation. Before the seams were introduced and the interpolation algorithms were applied, a 512×512 subarray was cropped.

4.2 *Impact of Seam Width*

In Table 6, the mean of the absolute and relative errors for each seam width was determined from all four images (refer to data in Tables 2–5). Clearly, the wider the seam is, the larger the errors are.

4.3 *Statistical Comparison of Adaptive Linear Interpolation and Conventional Linear Interpolation*

In a further comparison of the adaptive interpolation with the conventional linear interpolation, the following analysis was conducted. First, the differences of the two algorithms in terms of the relative errors and absolute errors were calculated, then the mean values of these differences were determined. The P values were also computed to show the significance of the comparison. As shown in Table 7, the mean of the differences are marginally larger than 0, which shows that the errors introduced by the adaptive interpolation are smaller than the errors introduced by conventional interpolation. The P values are 0.0000 for absolute errors and 0.0002 for relative errors, which verifies that the results of the comparison are statistically meaningful.[12]

Table 7 Comparison of adaptive and conventional linear interpolation, differences in errors and corresponding P values.

Difference	Mean	P value
1[a]	0.3035	0.0000
2[b]	0.004 175	0.0002

[a]Difference 1 is the absolute error induced by linear interpolation −absolute error induced by adaptive interpolation.

[b]Difference 2 is the relative error induced by linear interpolation −relative error induced by adaptive interpolation.

4.4 *Geometrical Distortion*

As demonstrated by quantitative comparisons with both relative and absolute errors, the adaptive interpolation is much better than the conventional linear interpolation for those features that are tilted with respect to the seam, such as the bone images of hand, forearm, wrist, etc. The superiority of the adaptive interpolation can also be observed by examining the geometrical distortion introduced by both interpolation algorithms. Figures 4(b)–6(b) show the enlarged portion of the original images of the hand bone and wrist bone. Figures 4(c)–6(c) show images with six-pixel seam width corresponding to Figs. 4(b)–6(b). Figures 4(d)–6(d) show the images interpolated with conventional linear algorithm. Noticeable geometrical distortion, as evidenced by discontinuity and misalignment at the location where the seam was, can be observed. In comparison, the "artifact" was less noticeable when the seam was interpolated using the adaptive algorithm, as demonstrated in Figs. 4(e)–6(e).

Experiments were also done on images with both vertical and horizontal seams. As expected, the adaptive algorithm gave better results, as shown in Figs. 7(c)–7(e).

4.5 *Comparison of the Adaptive Interpolation and Nonlinear Interpolation*

According to our previous studies,[11] the conventional linear interpolation offers similar accuracy with some other nonlinear algorithms, such as polynomial and cubic spline interpolations. This is, perhaps, due to the fact that the intensity distribution of radiographs is usually irregular. In other words, it is difficult to model a mathematical relationship between neighboring pixels in those images.

Table 7 shows that errors introduced by the adaptive algorithm are smaller than errors introduced by the conventional linear interpolation. The comparison results have also been proved to be statistically meaningful. Therefore, the adaptive algorithm should be better than some nonlinear algorithms, as shown in Figs. 7(f)–7(h).

Besides, adaptive interpolation is simpler and requires less computation. For example, in order to obtain Fig. 7(h), α was changed from $-\pi/3$ to $\pi/3$ with the speed of $\pi/5$. Approximately nine multiplication steps and six addition steps were needed to interpolate one pixel. However, in order to obtain Fig. 7(g), six pixels were used to interpolate one unknown pixel by the polynomial algorithm, in which 11 multiplication steps and six addition steps were used.

5 Discussion and Conclusion

In addition to the images demonstrated in this article, which were acquired by a lens coupled CCD, we did experiments on other images acquired by fiber optically coupled CCD. Overall, the adaptive interpolation offers better performance than that of the conventional interpolation algorithm for the images investigated. In terms of geometrical distor-

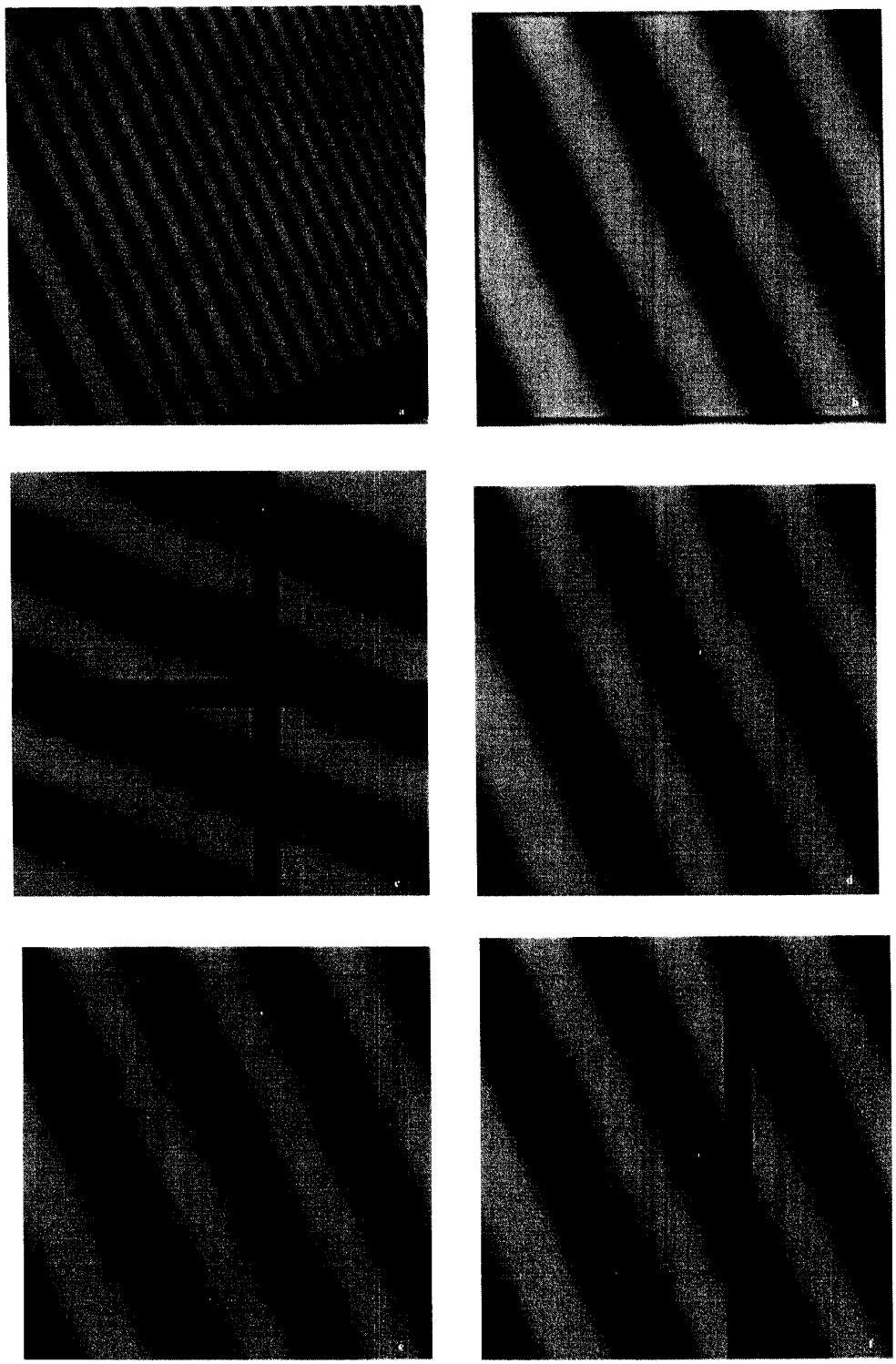

Fig. 7 This is an x-ray bar pattern image acquired with a lens-coupled CCD Prototype. The seams were introduced at 30° with respect to the lead bars: (a) original image with the portion to be enlarged in the rectangular block; (b) area of interest without seam (enlarged); (c) area of interest with six-pixels vertical and horizontal seam (enlarged); (d) area of interest reconstructed by linear local weighting interpolation (enlarged); (e) area of interest reconstructed by adaptive linear interpolation (enlarged); (f) area of interest with six pixel vertical seam (enlarged); (g) area of interest reconstructed by one dimensional polynomial interpolation (enlarged); (h) area of interest reconstructed by adaptive linear interpolation (enlarged).

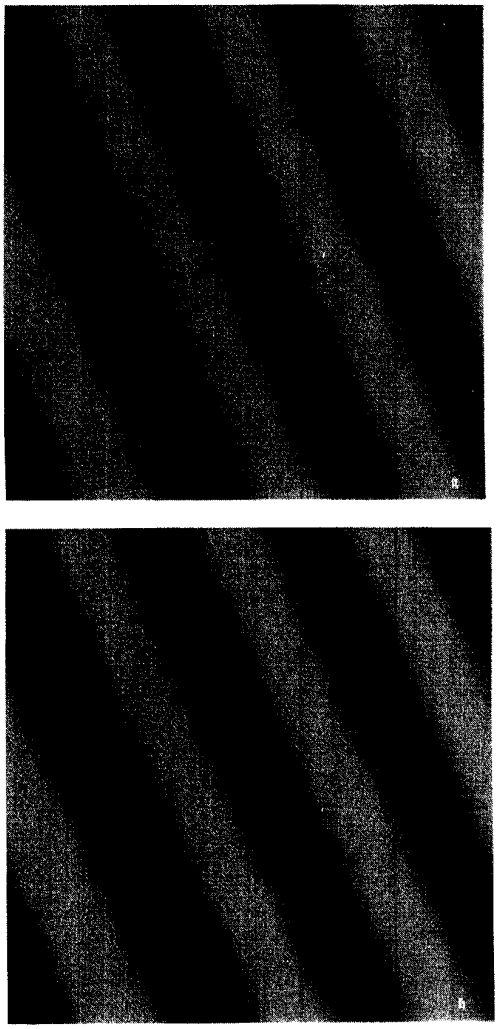

Fig. 7 Continued.

tion, the adaptive algorithm more closely assembles the clinically significant features and the associated noisy background. Quantitatively, the adaptive interpolation offers at least equivalent or less numerical error than that of the linear interpolation algorithm. The experimental results prove that there is a significant difference in both relative and absolute errors between two algorithms for tilted, high contrast features within an image, as exemplified by bone images. Furthermore, the seam width affects the accuracy of the interpolation significantly, so no matter which algorithm is used, the wider the seams are, the larger the errors are.

Ideally and when feasible, seams should be avoided in the design of digital radiography imaging systems. When seams do exist, well-designed interpolation is a practical solution for combining digital subimages.

The adaptive interpolation developed in this investigation is a simple linear algorithm. For the cases investigated in our experiments, we find that the adaptive linear interpolation is a useful technique for estimating missing information in the seam areas of digital radiographic images obtained using multiple digital detectors. Compared with some nonlinear algorithms, it is simple in mathematics and requires less computing time. Compared with conventional local weighting linear algorithms, it provides fewer errors.

Acknowledgments

This work was supported in part by PHHS Grants Nos. CA69043 and CA70209 by the National Cancer Institute.

References

1. G. S. Shaber, C. Lockard, and J. Boone, "High resolution digital radiography utilizing CCD planar array," *Proc. SPIE* **914**, 262–269 (1988).
2. A. Karellas, L. J. Harris, H. Liu, M. A. Davis, and C. J. D'Orsi, "Charge-coupled device detector: performance considerations and potential for mammographic imaging," *Med. Phys.* **19**(4), 1015–1023 (1992).
3. C. Kimme-Smith and T. Solberg, "Acceptance testing prone stereotactic biopsy units," *Med. Phys.* **21**(7), 1197–1201 (1994).
4. H. Liu, A. Karellas, L. Harris, and C. D'Orsi, "Optical properties of fiber tapers and their impact on the performance of a fiber optically coupled CCD x-ray imaging system," *Proc. SPIE* **1894**, 136–147 (1993).
5. H. Rochrig, L. L. Fajardo, Y. Tong, and W. V. Schempp, "Signal, noise and detective quantum efficiency in CCD based x-ray imaging systems for use in mammography," *Proc. SPIE* **2163**, 320–329 (1994).
6. H. Liu, A. Karellas, L. Harris, and C. D'Orsi, "Large-field high-spatial resolution digital x-ray mammography," *Proc. SPIE* **2390**, 110–115 (1995).
7. H. Liu, L. L. Fajardo, R. Baxter, J. H. Chen, J. McAdoo, G. Halama, and A. Jalink, "Full-size, high spatial resolution digital mammography using CCD scanning technique," in *Digital Mammography '96*, K. Doi, M. L. Giger, R. M. Nishikaw, and R. A. Schmidt, Eds., pp. 145–150, Elsevier, Amsterdam (1996).
8. M. J. Yaffe, "Digital mammography," in *Syllabus: A Categorical course in Physics Technical Aspects of Breast Imaging*, A. G. Haus and M. J. Yaffe, Eds., 2nd ed., pp. 271–282, RSNA (1993).
9. A. Jalink, J. McAdoo, G. Halama, and H. Liu, "CCD-Mosaic technique for large field digital mammography," *IEEE Trans. Med. Imaging* **15**(3), 260–267 (1996).
10. L. Chueng and R. Coe, "Full-field single-exposure digital mammography," *Med. Electron.*, (1995).
11. H. Liu, G. Wang, J. H. Chen, and L. L. Fajardo, "Interpolation algorithms for digital mammography systems using multiple detectors," *Academic Radiol.* (submitted).
12. B. Rosner, "Hypothesis testing: two-sample inference," in *Fundamentals of Biostatistics*, Chap. 7, pp. 253–256, Duxbury Press, Harrisonburg, VA (1995).